Characterization of low temperature high voltage axial insulator breaks for the ITER cryogenic supply line

IOP Conf. Series: Materials Science and Engineering **279** (2017) 012007 doi:10.1088/1757-899X/279/1/012007

Characterization of low temperature high voltage axial insulator breaks for the ITER cryogenic supply line

P Fernandez Pison[1,2], S Sgobba[1], I Aviles Santillana[1,2], S A E Langeslag[1], M Su[3], R Piccin[3], J Y Journeaux[3], A Laurenti[3] and W Pan[4]

[1] CERN, CH-1211 Genève, Switzerland
[2] University Carlos III of Madrid, Campus de Leganes, Av. Universidad 30, 28911 Madrid, Spain
[3] ITER Organization, Route de Vinon sur Verdon, CS 90 046 - 13067 St. Paul lez Durance cedex, France
[4] Institute of Plasma Physics, Chinese Academy of Sciences, Shushanhu 350, Hefei, 230031 Anhui, China

pilar.fernandez.pison@cern.ch

Abstract. Cable-in-conduit conductors of the ITER magnet system are directly cooled by supercritical helium. Insulation breaks are required in the liquid helium feed pipes to isolate the high voltage system of the magnet windings from the electrically grounded helium coolant supply line. They are submitted to high voltages and significant internal helium pressure and will experience mechanical forces resulting from differential thermal contraction and electro-mechanical loads. Insulation breaks consist essentially of stainless steel tubes overwrapped by an outer glass – fiber reinforced composite and bonded to an inner composite tube at each end of the stainless steel fittings. For some types of insulator breaks Glass – Kapton – Glass insulation layers are interleaved in the outer composite. Following an extensive mechanical testing campaign at cryogenic temperature combined with leak tightness tests, the present paper investigates through non-destructive and destructive techniques the physical and microstructural characteristics of the low temperature high voltage insulation breaks and of their individual components, thus allowing to correlate the structure and properties of the constituents to their overall performance. For all the tests performed, consistent and reproducible results were obtained within the range of the strict acceptance criteria defined for safe operation of the insulation breaks.

1. Introduction

New generation superconducting magnets for fusion projects, such as ITER, widely use coils based on technology of Cable-In-Conduit Conductors (CICCs) [1]. CICCs are designed based on various types of stainless steel jackets, densely filled with Nb_3Sn or NbTi superconducting strands, and subsequently compacted [2]. They are cooled by a forced flow of supercritical helium [3]. The magnet coils are directly connected to the helium supply pipes of the electrically grounded cryogenic distribution system.

In order to guarantee the electrical insulation between the helium supply pipes and the CICCs, Insulation Breaks (IBs) are used [4]. The IBs will be placed at the helium supply (inlets) and return points (outlets) of the different cryogenic circuits foreseen in the ITER magnet system. Depending on the operating environment of these cryogenic circuits, the IBs will withstand different potentials and

temperatures. A High-Voltage Low-Temperature (HVLT) IB will operate at 4.5 K and could experience a voltage difference of up to 28 kV in case of failure [4]. These HVLT IBs consist of stainless steel end-fittings overwrapped by an outer glass – fiber reinforced composite and bonded to an inner composite tube at each end of the stainless steel fittings. For some types of insulator breaks Glass – Kapton – Glass (GKG) insulation layers are interleaved in the outer composite (figure 1).

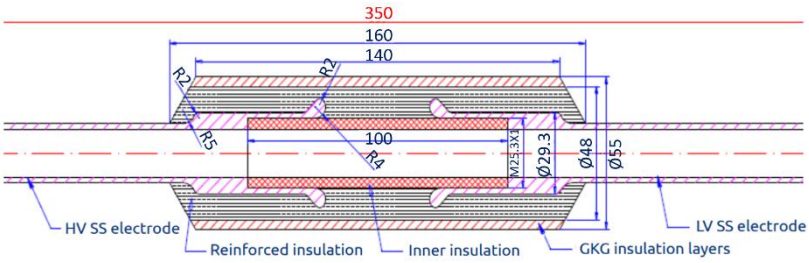

Figure 1. Schematic drawing of a HVLT IB (dimensions in mm), from [5].

In addition to the electrical potential and internal helium pressure that the IBs have to withstand at cryogenic temperature, they will also be submitted to a variety of mechanical forces resulting from differential thermal contraction and electro-magnetic loads [4]. Prior to the present assessment of the IBs, a characterization campaign aiming at testing their mechanical robustness was defined and executed. Mechanical testing at 77 K combined with leak tightness tests were carried out [5].

To further validate HVLT IBs against state of the art and specification requirements, an extensive assessment of the physical and microstructural characteristics of individual HVLT IBs and of their components have been performed. This comprehensive campaign addresses the material assessment of HVLT IBs for cryogenic use, which have already successfully passed prior qualification tests (mechanical, leak and high voltage tests). This campaign is aimed at confirming that IBs can withstand the highly demanding operating conditions in a cryogenic environment.

2. Components

Inspections were performed based on two identical 30 kV HVLT IBs (figure 1) identified as IBDH109 and IBDH251, respectively. Previous to the testing campaign reported here the two IBs were submitted to qualification tests. The latter included thermal cycling between room temperature (RT) and 77 K (100 thermal cycles), 4-point bend tests at RT, leak tightness tests, and high voltage electrical tests (partial discharge). Bearing this in mind, the IBs cannot be considered to be in a fully pristine state.

3. Experimental methods and results

An extensive characterization has been defined consisting of several reliability tests of individual IBs relevant for magnet operation. Destructive and non-destructive examinations included:

1. assessment of imperfections by visual and/or microoptical inspections in the axial and radial planes, and by die penetrant testing (PT);
2. measurement of the density of inner and outer ("reinforced") insulation composites (see figure 1), respectively;
3. assessment of the void fraction, fiber fraction and resin fraction of both insulation composites;
4. measurement of the fiber orientation;
5. assessment of the glass transition temperature (T_g) of the resin.

In order to evaluate the manufacturing quality of the inspected IBs for cryogenic use, they needed to be sectioned to access their internal structure. Firstly, sectioning along their axial center line was performed to obtain a flat finish and an exploitable surface for the analysis. One of the so obtained halves

was further sectioned in three portions, allowing one portion to be directly observed in a radial plane, and specimens from the inner and outer composites to be removed from the two other portions, respectively, for their individual assessment (figure 2).

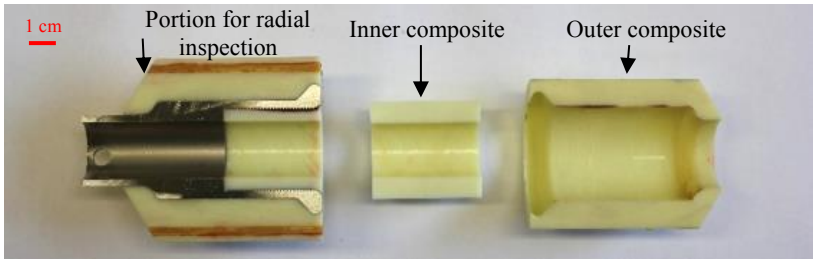

Figure 2. IBDH251 sectioned into three cross-sectional portions.

3.1. Assessment of imperfections
The destructive and non-destructive examinations applied for the assessment of imperfections are described hereafter.

3.1.1. Inspection in axial plane. The non-sectioned half of the individual IBs was microoptically inspected for any flaws in the structure (digital microscope VHX 1000E by KEYENCE). Since the cutting operation might have induced minor localized damage in the surface, such as slightly burnt regions in the composites, the surface was manually polished prior to the inspections. Figure 3 shows the state of IBDH251 prepared for the inspections.

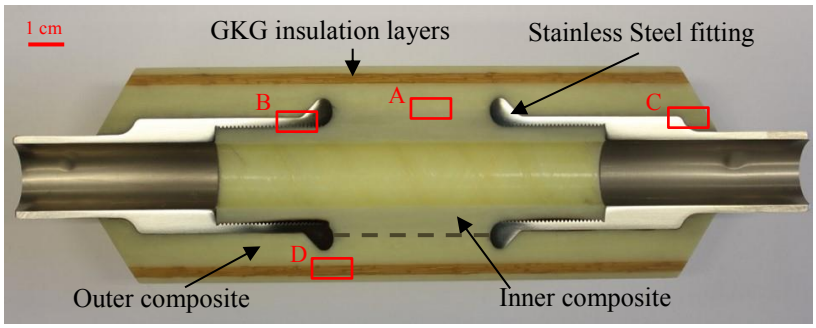

Figure 3. Longitudinal cut of IBDH251, showing the fields of view used for identifying specific features and their location. In fields of view A, B, C and D detailed observations were carried out.

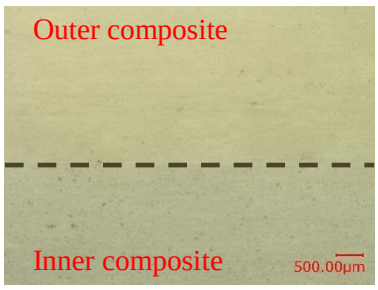

Figure 4. Interface between both composites; field of view A in figure 3.

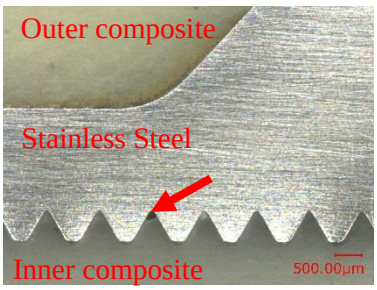

Figure 5. Void close to the stainless steel fitting; field of view B in figure 3.

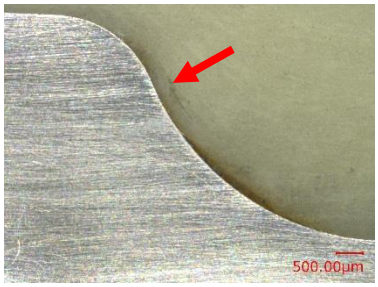

Figure 6. Cracks close to the stainless steel fitting; field of view C in figure 3.

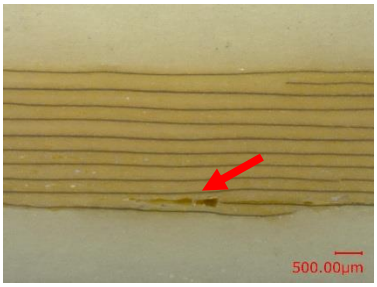

Figure 7. Voids in the GKG insulation layers; field of view D in figure 3.

For both IBs analyzed, a good continuity between the two composites was confirmed (figure 4, field A). No gross porosities were visible within the composites. However, in some regions around the stainless steel fittings, some voids and cracks were observed (figure 5, field B; and figure 6, field C). The GKG insulation layers showed some voids particularly concentrated towards the outer layer, more pronounced for IBDH251 than for IBDH109 (figure 7, field D).

3.1.2. Penetrant Testing (PT). Both halves of the individual IBs were examined by dye penetrant testing, Type II (visible dye) method A (water washable) according to ASTM E1417. PT was applied before performing further cross-sectional cuts. For both tested IBs, 20 minutes after the developer was applied (solvent-based white-powder penetrant developer), very pronounced linear indications were observed. They were mainly located at the stainless steel to composite interfaces and in the GKG insulation layers, which agree fairly well with the location of the imperfections observed in the axial inspection. The large amount of dye penetrant observed in some regions revealed deep discontinuities associated to the respective indications. Figure 8 shows the results obtained for IBDH109.

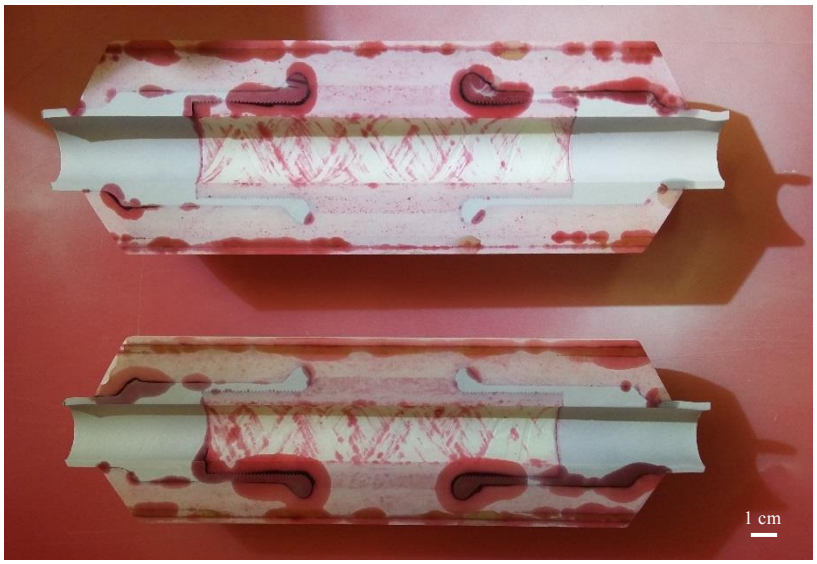

Figure 8. IBDH109 after application of developer. Dwell time: 20 minutes.

3.1.3. Inspection in radial plane. One cross-sectional portion of the individual IBs was used for the inspection. The radial plane was observed after manual polishing. For both IBs, small linear indications were observed in the stainless steel to composite interface. Long indications were found in the last layer of the outer GKG insulation (see figure 9 for IBDH251). Both cross sections were performed at the positions where major indications from PT performed in the axial plane were observed. Consistently, in these positions, the radial inspections have confirmed the presence and the extent of the imperfections already identified in the axial cut.

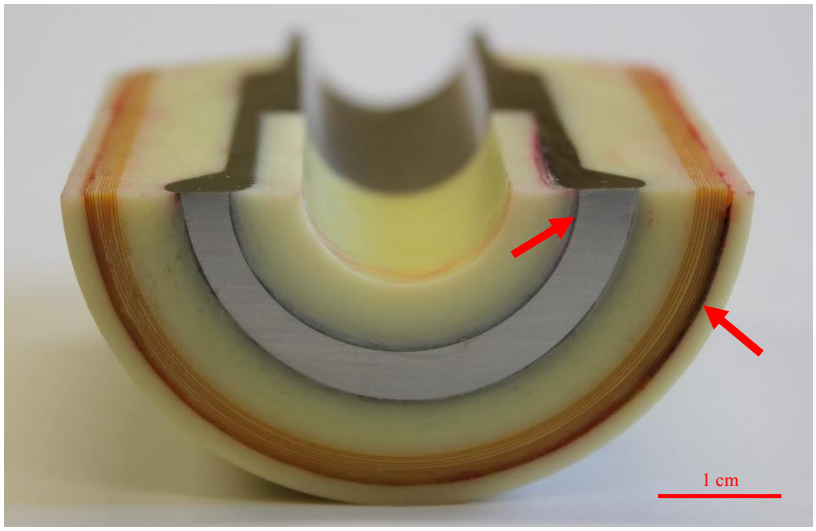

Figure 9. Radial inspection of IBDH251. The arrows show the indications already identified by PT on the axial cut, located in the stainless steel to composite interface and in the last layer of the GKG insulation layers, respectively.

3.2. Density

The density was measured in both inner and outer composites of the individual IBs, based on Archimedes' principle according to ASTM D792 (pure ethanol was used as the process fluid). Two specimens of approximately 5 g each, as required by the standard, for each composite were extracted from the two individual cross-sectional portions respectively (figure 2). The density was measured using a Sartorius analytical balance (accuracy class I). The specimens were measured three times for repeatability purposes. The results are shown in table 1 where similar densities for both IBs are observed.

Table 1. Summary results of densities for different components.

	IBDH109	IBDH251
Inner composite	1.88 g/cm^3 ± 0.01 g/cm^3	1.91 g/cm^3 ± 0.00 g/cm^3
Outer composite	1.86 g/cm^3 ± 0.01 g/cm^3	1.84 g/cm^3± 0.02 g/cm^3

3.3. Void, fiber and resin fraction

The assessment of the volume fraction of fiber, resin and void was performed according to ASTM D2584 (ignition loss method) on the same specimens used for the assessment of the density of the composites. Following weighing in an analytical balance the specimens were fired in a furnace at 550 ^{0}C for approximately 2 hours. Afterwards, they were cooled inside the furnace by natural convection and weighed again as soon as they reached RT. In order to confirm the complete removal of

the organic part of the composite material, an infrared spectroscopy analysis was carried out for one of the specimens of the outer composite of IBDH109, both before and after heat treatment. A full decomposition of the resin after 2 hours at 550 ^{0}C was confirmed. The results of the volume fractions are shown in table 2. It can be noticed that the void volume fraction of the outer composite of IBDH251 is slightly higher than the inner composite of the same IB and for both composites of IBDH109.

Table 2. Summary results of volume fraction of fiber, resin and void for different components.

	IBDH109			IBDH251		
	Vol. Fiber	Vol. Resin	Vol. Void	Vol. Fiber	Vol. Resin	Vol. Void
Inner composite	48.6 % ± 0.1 %	49.7 % ± 0.4 %	1.7 % ± 0.1 %	50.6 % ± 0.1 %	47.5 % ± 0.2 %	1.9 % ± 0.1 %
Outer composite	46.9 % ± 0.1 %	51.3 % ± 0.1 %	1.8 % ± 0.0 %	45.6 % ± 1.5 %	52.2 % ± 1.5 %	2.2 % ± 0.0 %

3.4. Fiber orientation

In order to estimate the fiber angle in the composites of the individual IBs, the specimens previously used for density and void fraction assessment were observed after combustion. The fired specimens were optically observed using a digital microscope (VHX 1000E by KEYENCE). The fiber angle was measured from the images using microscope specific image analysis software. It is important to note that only the fiber angle from the near surface layers visually accessible could be measured due to the fact that removing external layers of fibers to examine underlying fibers could modify the orientation of the latter, introducing errors. However, specimens for observation from both inner and outer diameter were prepared in order to investigate a possible change of the angle across the thickness. All of the composites show a braid pattern (figure 10). The braid angles measured with respect to the main axis (figure 11) are shown in table 3, similar values for each composite of both IBs were obtained.

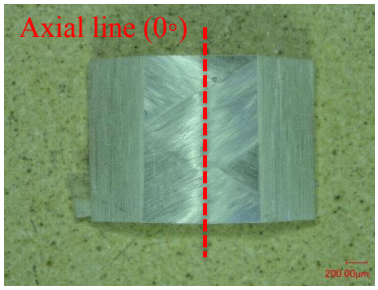

Figure 10. Inner composite of IBDH109 after firing.

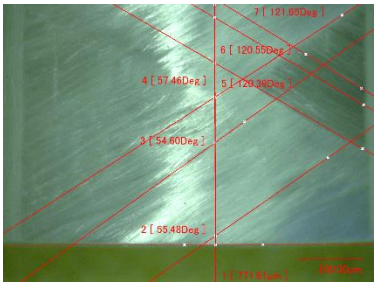

Figure 11. Fiber angle measurement for the inner composite of IBDH109.

Table 3. Summary results of braid angles, referred to the main axis, for different components.

	IBDH109	IBDH251
Inner composite	± 60.6º ± 3.3º	± 60.8º ± 2.2º
Outer composite	± 70.4º ± 3.1º	± 73.5º ± 4.4º

3.5. Glass transition temperature (T_g)

The evaluation of T_g of each of the two composites was performed according to IEC 61006 via Differential Scanning Calorimetry (DSC) using a SETARAM 131 calorimeter. For the measurement, 20 mg powder specimens from the two individual cross-sectional portions (figure 2), respectively, were obtained by ball milling and were warmed up with a ramp of 10 ^{0}C/min to a temperature of 200 ^{0}C under nitrogen. Measurement was repeated twice for each of the specimens, with an intermediate cool down (50 mL/min of pure nitrogen) to RT by forced convention. A third DSC analysis was carried out after the same intermediate cool down for the outer composite of IBDH109, in order to confirm the stabilization of T_g. The results for each of the composites for both IBs are displayed in table 4. An increment of T_g between the first and the second heating cycles is observed for both composites of both IBs. All specimens reach the same T_g (132 º ± 2 º) after the second heat cycle. The third DSC analysis showed no evolution in T_g.

Table 4. Summary results of T_g for different components.

	IBDH109			IBDH251		
	T_{g1}	T_{g2}	T_{g3}	T_{g1}	T_{g2}	T_{g3}
Inner composite	124 ºC	131 ºC	n.a.	122 ºC	134 ºC	n.a.
Outer composite	114 ºC	129 ºC	130 ºC	122 ºC	135 ºC	n.a.

4. Discussion

In both axial and radial planes several cracks and discontinuities were observed (figure 5 to figure 9), being of a considerable depth for most of them as revealed by PT. This confirms that although the observations were carried out in a single cross section per direction (axial and radial), the imperfections extend within the bulk. The most critical defects for both individual IBs were observed around the stainless steel fittings, towards the interface between them and the composites. Due to their axial orientation and their location, these discontinuities seem to have been induced by the hundred thermal cycles to liquid nitrogen to which the IBs were submitted prior to destructive examination. They are likely a consequence of high stresses induced by the difference in thermal expansion coefficient between the dissimilar materials. However, these cracks do not form a continuous network along the interfaces, and therefore they do not impair the strength and the leak tightness of the assembly [5]. Another critical region where imperfections were observed is the GKG insulation layers, which showed less soundness for IBDH251 compared to IBDH109. In general these imperfections present an ellipsoidal shape and did not evolve into long imperfections. They are generally small and their geometry is more favorable than elongated defects such as sharp cracks in terms of stress concentration.

The repeatability of the density results for the same IB is high, and in addition, similar densities were obtained for both IBs (table 1), meaning that during the fabrication, a stable process was achieved leading to homogeneous and dense composites.

Regarding the volume fraction of the different IBs for both composites, it is important to note that the void volume fraction of the outer composite of IBDH251 is slightly higher than the inner composite of the same IB and for both composites of IBDH109 (table 2). Moreover, the orientation of the fibers resulted in similar values for each composite of both IBs confirming repeatability and robustness of fabrication (table 3).

Based on the DSC results, an increment of T_g between the first and the second heating cycles was observed for both composites of both IBs (table 4). After the second heat cycle, all specimens reached the same T_g (132 ºC ± 2 ºC). The third DSC analysis showed no evolution in T_g after an additional heat cycle, confirming the stability of the obtained value. Based on these results, an incomplete polymerization of all studied composites is evident, which could be due to the high volume of the composite to be cured together with an expected low thermal conductivity of this type of material.

However, since both IBs successfully passed all tests included in the validation protocol, the impact of this fact is small. Moreover, an additional polymerization step will be carried out during assembly by an additional thermal cycle at 80 ºC.

The obtained results, together with previous tests confirming that IBs are leak tight against severe tensile loads at cryogenic temperature, represent a sufficient basis of qualification for their operation.

5. Conclusion

An in-depth characterization was successfully performed for the assessment of the physical properties and microstructure of HVLT IBs and of their individual components. Two individual IBs were assessed through non-destructive and destructive techniques.

Imperfections were observed by an axial and a radial inspection of the IBs and confirmed by PT. However, they proved not to impair the leak tightness within the range of design stresses at cryogenic temperature [5]. The properties of the bulk composites were assessed by measuring their respective density and calculating the volume fraction of fiber, resin, and void individually. Furthermore, the fiber orientation was measured through optical techniques, and T_g was determined via DSC. For all the tests performed, consistent and reproducible results were obtained.

To the extent of the investigations performed, the results are within the range of the strict acceptance criteria defined for safe operation of the IBs, therefore a reliable overall performance of the analyzed HVLT IBs is expected on this basis.

The views and opinions expressed herein do not necessarily reflect those of the ITER Organization.

References

[1] Mitchell N, Devred A, Libeyre P, Lim B and Savary F 2012 The ITER Magnets: Design and Construction Statud *IEEE Trans. Appl. Supercond.* **22** no. 3 4200809

[2] Turck B, Bessette D and Ciazynski D 1993 Design methods and actual performances of conductors for the superconducting coils of Tokamaks *Fusion Eng. Des.* **2** 667-70

[3] Bottura L and Luongo C 1999 Superconductors, stability in forced flow *Wiley Encyclopedia of Electrical and Electronics Engineering*

[4] Rodriguez-Mateos F, Evans D, Devred A, Laurenti A and Mitchell N 2014 Essential Design, Construction and Test Elements of ITER Axial Insulation Breaks *AIP Conf. Proc.* **1574** no.1 117-24

[5] Langeslag S A E, Rodriguez Castro E, Aviles Santillana I, Sgobba S and Foussat A 2015 Design of load-to-failure tests of high-voltage insulation breaks for ITER's cryogenic network *IOP Conf. Ser.: Mater. Sci. Eng.* **102** no.1, 012009

Acknowledgements

The cryogenic cycling, mechanical and electrical measurements and leak tightness tests were carried out by the Magnet Infrastructure Facilities for ITER (MIFI) under the supervision of the ITER Organization; T_g was measured by A. Rivière at the chemistry laboratory of CERN (TE/VSC/SCC); PT was performed by A.M. Piguiet, a level 2 certified operator (COFREND ID n° 012084) of the Materials and Metrology section of CERN (EN/MME/MM).